Comparing Eqs. (3) and (8) shows $F^{(1)}_{te1-si2} = F^{(2)}_{te1-si2}$ and, hence, completes the proof that the obstructing tube does not affect the view factor from a tube exterior surface to a shell interior surface. The view factors of configurations I and II are identical. Because an analytical solution for the view factor of configuration I has been provided by Howell,[4] the same can be used for configuration II. Figure 3 shows the comparison of the analytical solution (configuration I) with the numerical results of Reid and Tennant,[2] and the numerical results of Srinivasan and White[6] (both of configuration II). The indication that the analytical solution compares well with the numerical results supports the proof.

Concluding Remarks

The view factors for configurations I and II are proved to be identical. The view factors for configuration II, based on the analytical solution reported for configuration I, agree with the numerical results reported for configuration II. The analytical solution for configuration I can be used to obtain the view factor for configuration II.

Acknowledgment

The authors gratefully acknowledge the support provided by the National Science and Technology Board of Singapore, Project Number JTARC 5/96.

References

[1]Emery, A. F., Johansson, O., Lobo, M., and Abrous, A., "A Comparative Study of Methods for Computing the Diffuse Radiation Viewfactors for Complex Structures," *Journal of Heat Transfer*, Vol. 113, 1991, pp. 413–422.

[2]Reid, R. L., and Tennant, J. S., "Annular Ring View Factors," *AIAA Journal*, Vol. 11, No. 10, 1973, pp. 1446–1448.

[3]Rea, S. N., "Rapid Method for Determining Concentric Cylinder Radiation View Factors," *AIAA Journal*, Vol. 13, No. 8, 1975, pp. 1122, 1123.

[4]Howell, J. R., *A Catalog of Radiation Configuration Factors*, McGraw–Hill, New York, 1982.

[5]Shukla, K. N., and Ghosh, D., "Radiation Configuration Factors for Concentric Cylinder Bodies," *Indian Journal of Technology*, Vol. 23, 1985, pp. 244–246.

[6]Srinivasan, R., and White, A.C., "Analytical Expression for a Concentric-Cylinder Radiation View Factor," *Journal of Thermophysics and Heat Transfer*, Vol. 10, No. 3, 1996, pp. 534–536.

Effects of Contact and Spreading Resistance on Heat Sink Cooling Performance

J. G. Maveety*
Intel Corporation, Santa Clara, California 95052

Introduction

IN a system's environment, the junction temperature of a semiconductor device depends on the thermal resistance between the die, heat-sinking material, and ambient. To ensure the junction temperature will be maintained within a safe operating region, the thermal resistance must be reduced at the same rate that the power is dissipated. Consequently, understanding the contributors to the total thermal resistance helps in the design of thermal management.

In this work, experiments were conducted to investigate the effects of heat sink fin geometry and material selection on the cooling of a silicon test chip. The apparatus was instrumented so that the contributions to the total thermal resistance could be measured. Closed-form analytical expressions were used to predict the average thermal spreading resistance within the heat sink and the die-heat sink contact resistance.

Experiment Setup, Procedure, and Uncertainty Analysis

Two different heat sink pin arrays and materials were studied. Identical carbon composite and aluminum heat sinks were milled to have a square base measuring 50.8 × 50.8 mm. All of the fins were square and measured ($d \times d$). The fin-to-fin spacing, s, varied as the number of fins, n, were changed (see Table 1).

All heat sink contact surfaces were subjected to a grinding process that produced an rms surface roughness of 0.203 μm (8 μin.). The flatness of the heat sinks was 4 mil/in. The heat sinks were instrumented with four 36-gauge copper-constantan thermocouples. As shown in Fig. 1, one thermocouple, T_b, was placed 1.0 mm from the base, and the remaining three thermocouples, T_c, were placed 1.0 mm from the top of the heat sink base plate. The silicon thermal test chip has its own internal thermal diode that was used to measure the junction temperature, T_j. All measurements were collected using a NetDaq data-acquisition system.

The silicon test chip was an OLGA (organic land grid array) type, measuring 12 × 12 mm and capable of generating 30 W. The test chip was placed into an electrical contactor that was attached to an FR-4 load board. The setup is illustrated in Fig. 1. A dc power supply provided power input to the test chip. The contactor and load board were backed by a fiber-insulating board to minimize the heat loss through the bottom and sides of the apparatus. The heat sinks were placed on top of the test chip and loaded to give a constant die to sink contact force of 25 N for all experiments. This ensured good electrical contact between the test chip and contactor as well as good test chip to heat sink thermal contact. It is a well-documented fact that thermal contact resistance decreases with increased contact pressure; however, for OLGA packages, realistic limits of contact pressure are limited to ensure that solder joint attach and package surfaces are not damaged.

Steady-state air-impingement flow experiments were conducted with a round nozzle of diameter D = 6.4 mm. The results presented here were performed with $Re_D = 4.5 \times 10^4$.

Table 1 Fin numbers and spacing of arrays used in experiments[a]

$n \times n$	7 × 7	13 × 13
d	5.08	2.03
s	2.54	2.03

[a]Numerical values are in millimeters.

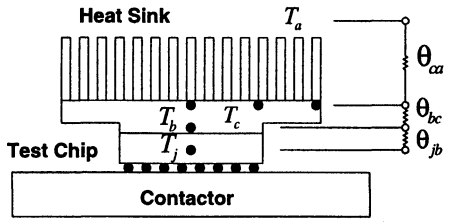

Fig. 1 Schematic of experimental setup. The thermal test chip is placed into an electrical contactor and the heat sink is placed on top of the test chip. Air is then impinged on the heat sink at $Re_D = 4.5 \times 10^4$.

Received March 18, 1998; revision received July 24, 1998; accepted for publication July 27, 1998.

*Santa Clara Processor Division, M/S RN3-61, 2200 Mission College Boulevard.

A methodical test procedure was followed in all experiments. For each data point, the flow rate and chip power were adjusted and the apparatus was allowed to reach steady state. Twenty-four repeatability studies were performed to validate the results presented here. A detailed uncertainty analysis was performed,[1] which showed $U(Re_D/Re_D) = 0.025$ and $U(\theta_{aa}/\theta_{ja}) = 0.033$ for the four heat sink geometries.

Analysis

The overall die junction-to-ambient steady-state thermal resistance values are used to measure the thermal performance of the heat sinks. This is defined by

$$R_{ja} = (T_j - T_a)/Q \tag{1}$$

where T_j is the die junction temperature, T_a is the ambient temperature, and Q is the power (heat) dissipated. Equation (1) can be split into the constituent thermal resistance parts that make up the junction-to-ambient total resistance. This is represented as

$$R_{ja} = R_{jb} + R_{bc} + R_{ca} \tag{2}$$

where R_{jb}, R_{bc}, and R_{ca} are the die-heat sink contact resistance, heat sink spreading resistance, and heat sink fin to ambient thermal resistances, respectively. R_{jb} is a measure of the temperature drop across two surfaces in contact. Contact resistance is a complicated interaction dependent on surface profiles, material hardness, mating pressure, and thermal conductivities. R_{bc} is a measure of the internal resistance within the heat sink base. This value is strongly dependent upon the heat sink material thermal conductivity and geometry. The thermal resistance between the heat sink to the ambient R_{ca} depends on heat sink geometry, airflow characteristics, as well as the package temperature.

Approximate analytical expressions that describe both the contact resistance and spreading resistance were used for comparison against the experimental data. The analytical model used to characterize the average internal spreading resistance was developed by Song et al.[2] The expression has the form

$$R_{bc} = \Psi_{av}/(\sqrt{\pi}ka) \tag{3}$$

where k is the thermal conductivity of the substrate, and $a = \sqrt{A_s/\pi}$ is the characteristic length scale, where A_s is the surface area of the heat source. The average dimensionless spreading resistance takes the form

$$\Psi_{av} = (\varepsilon\tau/\sqrt{\pi}) + \tfrac{1}{2}(1 - \varepsilon)^{3/2}\Phi_c \tag{4}$$

where

$$\Phi_c = \frac{\lambda_c + Bi\cdot\tanh(\lambda_c\tau)}{Bi + \lambda_c\cdot\tanh(\lambda_c\tau)} \tag{5}$$

$$\lambda_c = \pi + 1/(\sqrt{\pi}\varepsilon) \tag{6}$$

In the preceding equations, $\varepsilon = a/b$, $\tau = t/b$, where $b = \sqrt{A_b/\pi}$ and t is the base thickness. A_b is the spreader base area, and $Bi = hL/k$ is the Biot number, where L is the length of the heat sink base. Experimentally, the internal spreading resistance is defined as

$$R_{bc} = (T_b - \bar{T}_c)/Q \tag{7}$$

where $\bar{T}_c$ is the average heat sink fin base temperature.

Modeling contact resistance has been the focus of much attention, particularly when dealing with heat transfer through small surface area, high-power microdevices. As outlined in Refs. 3–6, the contributions to heat transfer across a two-layer interface can be split into two parts, conduction through the contact areas and conduction through the air gap voids.

The total contact conductance across a two-material interface is the sum of the contact conductance h_c and gap conductance h_g. As a result, the total heat transfer through the

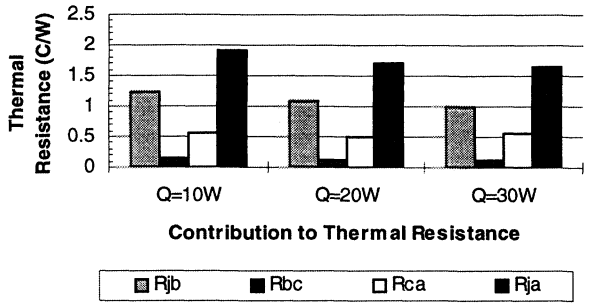

Fig. 2 Contributions to thermal resistance for the 13 × 13 aluminum heat sink (n = 13, Re = 45,000).

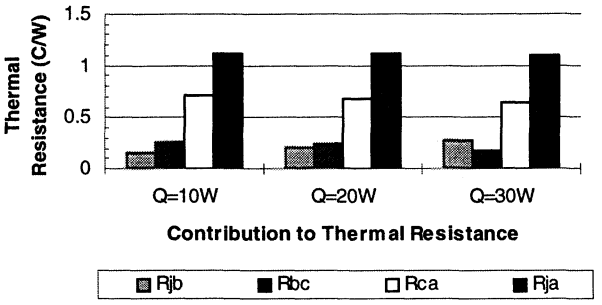

Fig. 3 Contributions to thermal resistance for the 13 × 13 composite heat sink (n = 13, Re = 45,000).

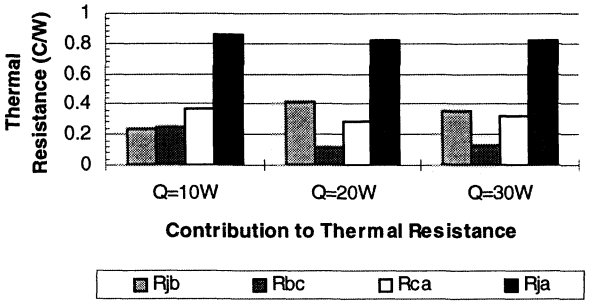

Fig. 4 Contributions to thermal resistance for the 7 × 7 aluminum heat sink (n = 7, Re = 45,000).

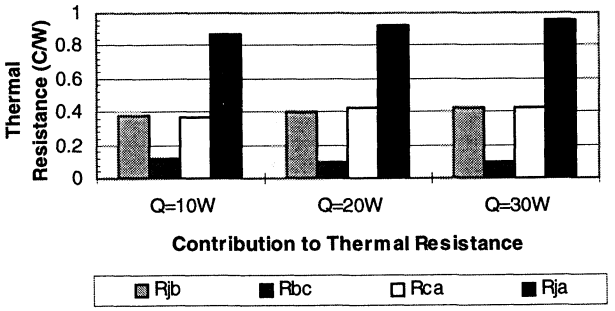

Fig. 5 Contributions to thermal resistance for the 7 × 7 composite heat sink (n = 7, Re = 45,000).

Table 2 Comparison between experimental and analytical values for spreading resistance within the base of the heat sinks[a]

Power dissipated, W	Aluminum 7 × 7	Composite 7 × 7	Aluminum 13 × 13	Composite 13 × 13
10 (experimental)	0.135	0.095	0.126	0.126
10 (analytical)	0.125	0.099	0.113	0.120
% error	7.40	5.30	10.30	4.76
20 (experimental)	0.115	0.99	0.113	0.099
20 (analytical)	0.125	0.99	0.113	0.099
% error	−8.70	0	0	0
30 (experimental)	0.120	0.090	0.108	0.100
30 (analytical)	0.125	0.090	0.113	0.099
% error	−4.20	0	−4.60	1.00

[a]Analytical values were computed using Eq. (3), experimental values were computed using Eq. (7). The resistance values are represented in °C/W.

interface can be separated into Q_c through the solid (contact) spots and Q_g through the gaps, such that

$$Q = Q_c + Q_g \tag{8}$$

Defining the solid spot conductance and gap conductance as $h_c = Q_c/(A\Delta T)$ and $h_g = Q_g/(A\Delta T)$, respectively, substitution into Eq. (8) gives

$$Q/A\Delta T = h_c + h_g \tag{9}$$

The reciprocal of the contact conductance given in Eq. (9) is the thermal resistance R_{bc} across the interface.

Antonetti et al.[7] developed a closed-form correlation to estimate the contact conductance through the contact areas in terms of the surface roughness, surface microhardness, thermal conductivity, and contact pressure. By eliminating the asperity slope in favor of using the average roughness, Antonetti et al. were able to obtain a correlation for the contact conductance that does not depend on asperity slope. The expression is

$$h_c = 4200k_sRa^{-0.257}(P/H)^{0.95} \tag{10}$$

In Eq. (10), $k_s = 2k_1k_2/(k_1 + k_2)$ is the harmonic mean thermal conductivity, $Ra = \sqrt{Ra_1^2 + Ra_2^2}$ is the combined average surface roughness, P is the contact pressure, and H is the surface hardness value of the softer material. h_c has the units W/m^{2}K, k_s is in W/mK, and Ra is in meters. The expression characterizing the gap void conductance is given by Madhusudana[8] as

$$h_g = k_g/(\delta + 2g) \tag{11}$$

where k_g is the thermal conductivity of the gas filling the gaps

$$\delta = 1.53Ra(P/H)^{-0.097} \tag{12}$$

$$g = [(2 - \alpha)/\alpha][2/(\gamma + 1)][k_g/(\mu C_v)]\lambda \tag{13}$$

where α is the accommodation coefficient (0.90),[7] γ is the ratio of specific heats for air, μ is the viscosity of air, C_v is the air specific heat at constant volume, and λ is the mean free path. The thermophysical property data used in the conductance calculations are as follows: $\mu = 18.5 \times 10^{-6}$ kg/m·s, $C_v = 718$ J/kg·K, $\lambda = 0.064 \times 10^{-6}$ m, $k = 200$ W/m·K, $k_g = 0.026$ W/m·K, thermal conductivity of composite (horizontal plane) = 600 W/m·K, thermal conductivity of composite (vertical) = 400 W/m·K, and $\alpha = 0.90$.

Table 3 Comparison between experimental and analytical values for contact resistance between die and heat sinks

	R_{jb}, °C/W	
Material	Experimental	Analytical
Aluminum	0.722 ± 0.40	0.602 ± 0.02
Composite	0.305 ± 0.11	0.204 ± 0.01

Results and Discussion

The contributions to total thermal resistance are presented separately and then the contact resistance and spreading resistance values are compared with those computed using the equations outlined earlier.

Figures 2 and 3 show the contributions to thermal resistance for the 13 × 13 aluminum and carbon-composite heat sinks for power settings of 10, 20, and 30 W. The airflow conditions were constant with $Re_D = 4.5 \times 10^4$. It is interesting to note that R_{jb} makes up more than 50% of the total thermal resistance for the aluminum heat sink, but is reduced to a factor of 20% for the composite. As a result of the high contact resistance of the aluminum heat sink, the temperature of the cooling fins is lowered, resulting in a low fin-to-ambient temperature difference, and subsequent low performance. The fact that the aluminum fins are much cooler than the composite fins, because of the high contact resistance of the aluminum heat sink, suggests that more heat is rejected through the load board.

Figures 4 and 5 show the contributions to thermal resistance for the 7 × 7 aluminum and composite heat sinks for the three power settings. Comparing the total performance R_{ja} between the 13 × 13 and 7 × 7 arrays, shows both 7 × 7 heat sinks to be superior in performance. Figure 4 shows that R_{jb} is the same order of magnitude as R_{bc} for the low-power setting, but is larger than both R_{bc} and R_{ca} for higher power settings. This indicates that although optimizing a fin geometry is important, the effects of contact resistance can contribute as much as 50% of the thermal impedance.

Figures 2–5 show that the junction to base contact resistance R_{jb} does not change appreciably with changes in the power range investigated here. This is expected because there are no physical phenomena that change sufficiently enough to appreciably alter the convection heat transfer from the fins. Consequently, the variation in R_{jb} for the power settings selected are attributed to experimental uncertainties.

Both analytical and experimental results for average heat sink spreading resistance are summarized in Table 2. The tabulation was generated for the constant forced convective flow $Re_D = 4.5 \times 10^4$, with three power settings 10, 20, and 30 W. The composite and aluminum heat sinks exhibit a decrease in spreading resistance with increased power. This is a result of a smaller temperature difference within the heat sink, even though the heat sink is operating at a higher mean temperature. The analytical and experimental results agree in general within 11%.

The comparison of the analytical contact conductance model[7,8] to describe R_{jb} and the experimentally obtained values is shown in Table 3. Uncertainty in the parameters used in the analytical model was estimated to be 3.5%, and the error associated with the experimental values was computed using a 95% confidence interval. However, it is not uncommon for hardness to vary ±10% for essentially homogeneous materials such as aluminum. Hardness of heterogeneous materials, such as carbon composite, may vary greatly, depending upon the number and depth of fibers below the surface.

The summary presented in Table 3 shows a considerable decrease in the composite contact resistance to that of aluminum. This could be attributed to aluminum oxide that could have formed. Although not confirmed, the decrease in contact resistance with the composite could be attributed to composite fibers coming in contact with the die surface, allowing for more conduction paths.

Conclusions

Experiments were performed to investigate the effects of contact and spreading resistance as applied to the cooling of an OLGA package. There were two types of heat sinking materials used, aluminum and carbon composite. The composite material proved to have higher overall performance, as measured by the lower overall junction-to-ambient thermal resistance. Closed-form analytical expressions characterizing contact resistance and spreading resistance were shown to be accurate in predicting both heat transfer processes, even though the analytical models were not calibrated using composite material.

Heat transfer across an interface is complex because the thermal resistance can depend on many geometric, thermal, and mechanical parameters. Separating the overall thermal resistance into constituent components allows for comparison of the contributions. The experiments presented here show that the interface contact resistance can account for as much as 50% of the total thermal resistance. The results presented here imply that we cannot ignore the effects of contact resistance in the application of electronic cooling. As die and packages continue to decrease in size, and power dissipation continues to increase, the contact resistance and thermal spreading processes will only be exacerbated.

References

[1]"Part 1 Measurement Uncertainty—Instruments and Apparatus," ANSI/ASME PTC 19.1-1985, American Society of Mechanical Engineers, New York, 1986.

[2]Song, S., Lee, S., and Au, V., "Closed-Form Equation for Thermal Constriction/Spreading Resistances with Variable Resistance Boundary Condition," *Proceedings of the 1994 International Electronics Packaging Conference* (Atlanta GA), 1994, pp. 111–121.

[3]Fletcher, L. S., "Recent Developments in Contact Conductance Heat Transfer," *Journal of Heat Transfer*, Vol. 110, 1988, pp. 1059–1070.

[4]Lambert, M. A., and Fletcher, L. S., "Review of the Thermal Contact Conductance of Junctions with Metallic Coatings and Films," *Journal of Thermophysics and Heat Transfer*, Vol. 7, No. 4, 1993, pp. 547–554.

[5]Madhusudana, C. V., and Fletcher, L. S., "Contact Heat Transfer—The Last Decade," *AIAA Journal*, Vol. 24, No. 3, 1985, pp. 510–523.

[6]Yovanovich, M. M., and Antonetti, V. W., "Application of Thermal Contact Resistance Theory to Electronic Packages," *Advances in Thermal Modeling of Electronic Components and Systems*, edited by A. Bar-Cohen and A. D. Kraus, Vol. 1, 1988, pp. 79–128.

[7]Antonetti, V. W., Whittle, T. D., and Simons, R. E., "An Approximate Thermal Contact Conductance Correlation," *Journal of Electronic Packaging*, Vol. 115, 1993, pp. 131–134.

[8]Madhusudana, C. V., *Thermal Contact Conductance*, Springer–Verlag, New York, 1996, pp. 1–61.

Experimental and Numerical Study of Thermovibrational Convection

R. Monti,* R. Savino,† and G. Alterio‡
University of Naples, Piazzale Tecchio 80-80125, Naples, Italy
and
R. Fortezza§
Microgravity Advanced Research and Support Center, Via Comunale Tavernola, 80144 Naples, Italy

Nomenclature

b = displacement, cm
f = frequency, Hz
g_0 = acceleration of gravity, 981 cm/s^2
H = vertical length (along y axis), cm
L = horizontal length (along x axis), cm
Pr = Prandtl number, ν/α
Ra_g = gravitational Rayleigh number, $g\beta_T\Delta TL^3/\nu\alpha$
Ra_v = vibrational Rayleigh number, $(b\omega\beta_T\Delta TL)^2/2\nu\alpha$
T = temperature, K
α = thermal diffusivity, cm^2/s
β_T = thermal expansion coefficient, K^{-1}
ΔT = temperature difference, K
μ = dynamic viscosity, g cm^{-1} s^{-1}
ν = kinematic viscosity, cm^2/s
ρ = fluid density, g/cm^3
ω = angular frequency, s^{-1}

Introduction

THE phenomenon of thermovibrational convection has been extensively investigated in Russian literature.[1–3] In the pioneering theoretical studies of Gershuni and Zhukhovitskii,[1] the influence of high-frequency vibrations on the behavior of liquids, in the presence of a thermal gradient, was studied by time-averaging the fluid dynamic equations. One of the most important results of these studies was that vibrations of a fluid cell, in the presence of temperature gradients, may induce a convective flow that, in turn, distorts the temperature distribution, compared with the purely diffusive situation. The experimental results obtained by Zavarykin et al.[2,3] confirmed the existence of thermovibrational convection in a liquid vibrating in the presence of a temperature gradient in Earth's gravity field.

The present authors point out that these effects may be particularly important during fluid and material science microgravity experimentation on the International Space Station,[4] where the residual gravity is reduced by several orders of magnitude and high-frequency g-jitter may be sources of acceleration disturbances. The study of thermovibrational effects on fluid and material science experiments is of primary importance, for the appropriate planning of the space activities and for the postflight analysis of the results obtained.

Recent theoretical and numerical studies in this field[5,6] have shown that, in the range of frequencies of interest for the space

Received Jan. 26, 1998; revision received Aug. 3, 1998; accepted for publication Aug. 6, 1998.

*Professor of Aerodynamics, Dipartimento di Scienza e Ingegneria dello Spazio "Luigi G. Napolitano." E-mail: monti@unina.it. Member AIAA.

†Researcher, Dipartimento di Scienza e Ingegneria dello Spazio "Luigi G. Napolitano." E-mail: rasavino@unina.it.

‡Ph.D. Student, Dipartimento di Scienza e Ingegneria dello Spazio "Luigi G. Napolitano."

§Researcher. E-mail: fortezza@mars.unina.it.